



HAL
open science

The shape and speciation of Ag nanoparticles drive their impacts on organisms in a lotic ecosystem

Melanie Auffan, Catherine Santaella, L Brousset, M Tella, E Morel, P Ortet, M Barakat, C Chaneac, J Issartel, B Angeletti, et al.

► To cite this version:

Melanie Auffan, Catherine Santaella, L Brousset, M Tella, E Morel, et al.. The shape and speciation of Ag nanoparticles drive their impacts on organisms in a lotic ecosystem. *Environmental science.Nano*, 2020, 7, pp.3167 - 3177. 10.1039/d0en00442a . hal-03065323

HAL Id: hal-03065323

<https://amu.hal.science/hal-03065323>

Submitted on 23 Aug 2021

HAL is a multi-disciplinary open access archive for the deposit and dissemination of scientific research documents, whether they are published or not. The documents may come from teaching and research institutions in France or abroad, or from public or private research centers.

L'archive ouverte pluridisciplinaire **HAL**, est destinée au dépôt et à la diffusion de documents scientifiques de niveau recherche, publiés ou non, émanant des établissements d'enseignement et de recherche français ou étrangers, des laboratoires publics ou privés.

The shape and speciation of Ag nanoparticles drive their impacts on organisms in a lotic ecosystem

M. Auffan^{*a, b}, C. Santaella^c, L. Brousset^d, M. Tella^e, C. E. Morel^a, P. Ortet^c, M. Barakat^c, C. Chaneac^f, J. Issartel^d, B. Angeletti^a, C. Levard^a, J-L. Hazemann^g, M. Wiesner^b, J. Rose^{a, b}, A. Thiéry^d, J.-Y. Bottero^{a, b}

^a CEREGE, CNRS, Aix Marseille Univ, IRD, INRAE, Coll France, Aix-en-Provence, France

^b CEINT Center, Duke University, Durham, NC 27708, USA

^c Aix Marseille Univ, CEA, CNRS, LEMIRE, 13108 Saint-Paul-lez-Durance, France

^d Aix-Marseille Univ, Univ Avignon, CNRS, IRD, IMBE, Marseille, France

^e CIRAD, US Analyse, F-34398 Montpellier, France, Analyse, Univ Montpellier, CIRAD, Montpellier, France

^f Sorbonne Université, CNRS, Collège de France, LCMCP, France

^g CNRS, Institut Néel, Université Grenoble Alpes, Grenoble, France

Electronic Supplementary Information (ESI) available: [supplementary physico-chemical characterization of NMs and microbiota analysis]. See DOI: 10.1039/x0xx00000x

Silver nanomaterials with different shapes (spheres, plates, wires, rods, cubes) are valued by industries and scientists for their shape-dependent properties which make them useful for diverse applications. In a safer-by-design perspective, controlling the shape of Ag nanomaterials could be an option to increase their potential applications while lowering either their hazard or their exposure potentials. Nine indoor aquatic mesocosms reproducing a lotic ecosystem were contaminated with chronic low-level additions of Ag nanospheres (Sp-Ag) and nanoplates (Pl-Ag) during a month. A shape-dependent impact in such environmentally relevant exposure conditions was observed. Pl-Ag induced a moderate oxidative stress in adult *Gammarus fossarum* (after molt) and an hormesis effect in the planktonic microbial communities, while Sp-Ag had no effect. In an environmental risk perspective, our results highlight which ecological niches of a lotic ecosystems would be more impacted by Pl-Ag : (i) >72% of the total Ag was found fully sulfidized in surficial sediment and had only moderate impact on benthic macro-organisms, (ii) only 11 to 15% of the Ag remained in the water column after 1 month, but Ag was under a more reactive speciation that impacts significantly the planktonic community.

1 Introduction

2 Controlling the size, shape, and structure of metal-based nanomaterials (NM) is technologically important
3 due to the strong correlation between the intrinsic properties of NMs and their potential applications^{1, 2}.
4 For instance, silver nanomaterials (nanospheres, triangular nanoplates, nanowires, nanorods, or
5 nanocubes) are valued by industries and scientists for their size- and shape-dependent properties which
6 make them useful for diverse applications as optics, catalysis, sensors, antimicrobial agents, etc.^{3, 4}. Silver
7 nanospheres are commonly used in antibacterial and antifungal applications, silver nanoplates in analytical
8 chemistry as optical sensors, and silver nanowires as promising conductive films for flexible touch screens<sup>5-
9 7</sup>. One reason for the particularities of these applications stems from the relationship between nanoparticle
10 shapes and the associated crystallographic faces exhibited that may allow for the tuning of surface
11 reactivity and bulk properties. For instance, silver nanocubes have the {100} crystal faces as basal plane,
12 whereas truncated triangular nanoplates and near-spherical nanoparticles predominantly exhibit the
13 most-stable {111} crystal face. Also, for a given mass, a spherical geometry minimizes surface area. As a
14 result, the rate of the reaction (in catalytic oxidation) of nanocubes is >14 times higher than nanoplates
15 and 4 times higher than nanospheres⁸.
16 Despite the challenge of controlling the shape of NMs during synthesis, several questions have been raised
17 regarding the potential shape-dependence of hazard and exposure posed by NMs. George et al. (2012)
18 studied the impacts of Ag nanospheres, nanoplates, and nanowires toward a fish gill cell line and zebrafish
19 embryos (doses tested 0.39-25 mg.L⁻¹). For both organisms, Ag nanoplates were significantly more toxic
20 due to a high level of crystal defects (stacking faults and point defects) on the nanoplate surfaces⁹. Pal et
21 al. (2007) also observed that truncated triangular silver nanoplates displayed the strongest biocidal action
22 (doses tested 0.01-10 mg.L⁻¹) toward *Escherichia coli*¹⁰. This was attributed to the high atom density
23 {111} facet of the basal plane. Tak et al. (2015) assessed the penetration rates and depths through
24 different layers of skin (*in vitro* and *in vivo*) of Ag nanospheres, nanorods and nanoplates¹¹. Ag nanorods
25 had the highest penetration and accumulated in the dermal layer, while triangular nanoplates had a slower

1 penetration capability. Even if the mechanisms beyond these differences were not fully understood, such
2 a shape-dependence allowed determining the therapeutic potential of Ag NMs *versus* their systemic
3 toxicity¹¹.

4 From a safer-by-design perspective, the risk related to nanomaterials for both human and the environment
5 may be mitigated by lowering either the hazard or the exposure potential¹². Controlling the shape of Ag
6 NMs could be an option to fine-tune their efficacy in specific applications while reducing their potential
7 harmful effects once release in the Environment. To our knowledge, such a shape-effect has never been
8 assessed towards freshwater ecosystems under realistic exposure scenario.

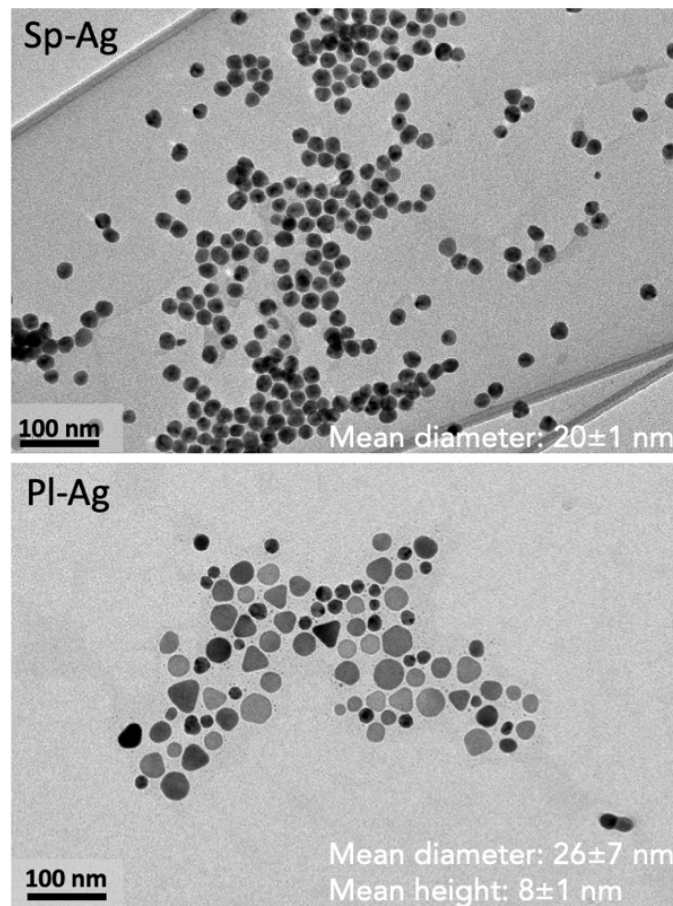
9 Herein, we designed indoor aquatic mesocosm experiments to compare the environmental behavior, fate,
10 and impact of Ag NMs with different shapes (plate and sphere) and consequently contrasted surface
11 reactivities. Such mesocosm testing provides meaningful data to inform about environmental risk toward
12 ecosystems¹³⁻¹⁶. A mesocosm is define here as an enclosed and, essentially self-sufficient (but not
13 necessarily isolated) experimental environment or ecosystem with a number of interdependent system
14 parameters¹⁷. Mesocosm experiments allow answering two research questions. First, do the shape-
15 dependent biological effects of Ag NMs previously observed *in vitro* on cell lines and *in vivo* toward mice
16 also observed toward freshwater ecosystems under a realistic exposure scenario (chronic low-level
17 additions of Ag, mid-term exposure)? Second, how the impacts towards benthic and planktonic ecological
18 niches of a lotic ecosystem differ following exposure to these Ag NMs and their degradation byproducts?
19 Nine indoor aquatic mesocosms reproducing a lotic ecosystem were dosed with chronic low-level additions
20 of Ag nanospheres (Sp-Ag) and triangular nanoplates (PI-Ag) during one month (final concentration of 42
21 and 47 $\mu\text{g}\cdot\text{L}^{-1}$ respectively). The biological impacts were assessed on the freshwater benthic detritivore
22 *Gammarus fossarum* (*Crustacea Amphipoda*) through the analysis of oxidative stress biomarkers, and on
23 microbial communities by pyrosequencing of the 16S rRNA gene. The (bio)distribution and
24 (bio)transformation were assessed by inductively coupled mass spectrometry and X-ray absorption
25 spectroscopy. *G. fossarum* is a detritivore crustacean with a key role in stream ecosystems (e.g. involved in
26 leaf litter breakdown process, predated by other macroinvertebrates, fishes and amphibians)¹⁸ and has
27 been extensively used as a pertinent model organism for the ecotoxicity evaluation of a contaminants.
28 Herein, the final concentration of exposure to PI-Ag and Sp-Ag is in the lower ranger of the LC50 previously
29 determined for gammarids (between 5 to 1000 $\mu\text{g}\cdot\text{L}^{-1}$)¹⁹.

30 **Materials and methods**

31 **Spherical and triangular plate Ag nanoparticles suspensions**

32 Polyvinylpyrrolidone coated spherical (Sp-Ag) and triangular plates (PI-Ag) silver NMs suspensions were
33 purchased from Nanocompositix[®]. The commercialized stock suspensions were stored at 4°C for less than
34 one month at 21.23 $\text{mg}\cdot\text{L}^{-1}$ (Sp-Ag) and 20.77 $\text{mg}\cdot\text{L}^{-1}$ (PI-Ag). The amount of dissolved Ag in the stock
35 suspensions were measured by ICP-MS (Nexlon 300X[®], Perkin Elmer) after ultracentrifugation (at
36 396 750xg for 1 h) at ~3.7% (Sp-Ag) and ~0.2% (PI-Ag). The suspensions were then dialyzed (10 KDa) in
37 milliQ[®] water to homogenize these amounts to $0.3 \pm 0.1\%$ (percentage of dissolved Ag vs total Ag). After
38 dialysis the conductivity of the suspensions were 53 $\mu\text{S}\cdot\text{cm}^{-1}$ for PI-Ag and 2.2 $\mu\text{S}\cdot\text{cm}^{-1}$ for Sp-Ag.

39 Observations of particles have been carried on a FEI Tecnai Spirit G2 TEM (Transmission Electron
40 Microscope) working with an acceleration voltage of 120 kV. For the analysis, one drop of particle
41 suspension is deposited on a carbon film coated copper grid. The average diameter of Sp-Ag was 20 ± 1 nm,
42 while PI-Ag had a mean diameter of 26 ± 7 nm and mean height of 8 ± 1 nm (Fig. 1). Based on the TEM sizes
43 and shapes, the specific surface area (SSA) were estimated at 25 ± 3 $\text{m}^2\cdot\text{g}^{-1}$ (Sp-Ag) and 29 ± 13 $\text{m}^2\cdot\text{g}^{-1}$ (PI-Ag).
44 The metallic Ag(0) composition of the Sp-Ag and PI-Ag was confirmed by Ag K-edge X-ray Absorption Near-
45 Edge Structure (XANES) (Figure S1). Both suspensions have a zeta potential between -20 and -15 mV from
46 pH 3 to 9 due to the PVP coating and average hydrodynamic diameter of 21 ± 3 nm (Sp-Ag) and 24 ± 3 nm
47 (PI-Ag) measured by dynamic light scattering (DLS) and electrophoretic mobility (Zeta nanosizer,
48 Marlvern[®], UK) (Figure S1).



1

2

Fig. 1 Size and shape of the Pl-Ag and Sp-Ag nanoparticles in their stock suspensions. TEM images and average particles sizes \pm standard deviation.

3

4 **Mesocosm set-up and monitoring**

5

Nine indoor mesocosms (glass tanks of 750×200×600 mm) were set up to mimic a natural river. Natural sediments and organisms were collected from a non-contaminated river in southern France (43.81138 N, 5.34399 E, altitude 294 m a.s.l.). Each mesocosm consisted of a layer of artificial sediment (89% SiO₂, 10% kaolinite, 1% CaCO₃) covered with 240 g of water-saturated natural sediment (sieved <200 μm) containing primary producers (*e.g.*, algae, bacteria), and 46 L of Volvic® water. The depth of the sediments was ~5 cm and the height of the water column was ~50 cm. The pH and conductivity values of the Volvic® water were close to those of natural river water. The natural water parameters registered the day of field sampling were 11.4° C, 95.6 % O₂ *i.e.* 10.12 mg.L⁻¹, 435 μS.cm⁻¹, and pH 8.11. See Auffan et al. (2014) for more details on the mesocosm set-up and monitoring¹⁶.

10

11

12

13

14

The mesocosms were operated over an initial equilibration period of nine weeks at which point they were considered to be at steady state as measured by stable values of the physico-chemical parameters (pH, oxidation-reduction potential (ORP), dissolved O₂, temperature, conductivity, and turbidity) in the mesocosms and the development of the primary producers. After the equilibration period, 100 adult amphipods *G. fossarum* (Koch, 1836) were introduced in each mesocosm. Only adults were brought in the mesocosms but birth occurred during the experiments. Two days after the organism introduction, three mesocosms were dosed with Sp-Ag, three with Pl-Ag, and three were kept as controls.

18

19

20

21

22

23

24

25

26

27

28

Details on the parameters monitored are provided in Figure S2. Briefly, temperature (15.3±0.6°C), dissolved oxygen (10.6±0.6 mg.L⁻¹), pH (8.0±0.1), and electrical conductivity corrected at 25°C (276±17 μS.cm⁻¹) were constant over time. The water column was oxidative (218±53 mV), while reductive conditions prevailed in sediments (-187±117 mV) (Figure S2). The concentration of phosphates and carbonates were 3.8×10⁻⁶ mol.L⁻¹ and 0.2×10⁻³ mol.L⁻¹ respectively in controls after 4 weeks. The primary producers were counted weekly in both water column and sediments. The concentrations of picoplankton and algae were respectively between 10⁴-10⁷ cells.mL⁻¹ and 10²-10⁴ cells.mL⁻¹ in the water column and between 10⁷-10⁸ cells.mL⁻¹ and 10⁶-10⁷ cell.mL⁻¹ in surficial sediments (Figure S3). The concentration of

1 colloidal particles ($<0.7\mu\text{m}$) in the water column was constant over time around 10^6 particle. mL^{-1} as
2 measured using the optical counter Flowcell® FC200S+HR (OCCHIO).

3 **Aquatic mesocosms dosing**

4 Starting at Day 0 (2 days after introduction of the organisms), the water column of respective mesocosms
5 was dosed 3 times per week (on Monday, Wednesday, and Friday) with PI-Ag or Sp-Ag during 28 days. The
6 total and dissolved [Ag] were measured in dialyzed stock suspensions prior to each dosing. Since SSAs of
7 Sp-Ag and PI-Ag were not statistically different, mesocosms were dosed with similar mass- and surface
8 area-based concentrations. The final [Ag] obtained after 4 weeks were $46.8\ \mu\text{g.L}^{-1}$ *i.e.* $1.4(\pm 0.6)\times 10^{-3}\ \text{m}^2.\text{L}^{-1}$
9 for PI-Ag and $42.1\ \mu\text{g.L}^{-1}$ *i.e.* $1.1(\pm 0.1)\times 10^{-3}\ \text{m}^2.\text{L}^{-1}$ for Sp-Ag.

10 **Distribution in the mesocosms**

11 The Ag content was measured by ICP-MS (Nexlon 300X®, Perkin Elmer) in sediment, water column, and
12 organisms (adults and juveniles *G. fossarum*). Surficial sediments (depth of sampling estimated at about
13 $0.9\pm 0.4\ \text{cm}$)¹⁵, water column (at $\sim 10\ \text{cm}$ from the air/water interface), and adult *G. fossarum* were sampled
14 at Day 7, 14, 21, and 28. At Day 28, cores of sediment were sampled as well as juvenile *G. fossarum*. Each
15 sampling of water, sediment and organism was performed in triplicate (sampling randomly distributed in
16 one tank) and pooled for chemical analysis. The data presented are the average and standard deviation
17 obtained within 3 replicated mesocosms.

18 Dialysis bags (10 kDa) filled with milliQ water were also placed in the water tank before NMs input, and 5
19 mL were once a week extracted from the bags for dissolved Ag analysis.

20 All samples were acid digested before ICP-MS analysis using adapted protocols²⁰. The measurement quality
21 was controlled using certified reference materials (HISS-1 marine sediment reference, CRM-NRC) and
22 homemade references. All Ag concentrations expressed in mg.kg^{-1} correspond to dry weight.

23 **Structural analysis**

24 Silver K-edge (25.514 KeV) XANES spectra were acquired at the European Synchrotron Radiation Facility
25 (ESRF, France) on the FAME beamline (BM30b) with Si(220) monochromator crystals^{21, 22}. Prior analysis,
26 sediment and organisms were freeze-dried and pressed into pellets. Spectral acquisition was performed at
27 liquid helium temperature to avoid sample evolution under the beam. Measurements were carried out in
28 fluorescence mode using a Canberra Ge solid-state detector. Each spectrum was at least the sum of three
29 scans. Data reduction was performed using the *Iffeffit* software package²³. Sp-Ag, PI-Ag, Ag₂S, Ag-GSH were
30 used as reference compounds.

31 **Lipid peroxidation and total antioxidant capacity measurements**

32 Between 6 to 8 adult *G. fossarum*, pooled from the three mesocosms of each condition, were sampled at
33 days 14, 21 and 28. Immediately after sampling, organisms were gently dried on towel paper and frozen in
34 liquid nitrogen. Samples were stored at -80°C until the start of the assays. Gammarids were individually
35 crushed using a MM 400 homogenizer (Retsch®, Germany) in 350 μL of extraction buffer (5 mM KH₂PO₄,
36 pH 7.4 with 0.9 % NaCl and 0.1% glucose). Homogenized samples were then used for lipid peroxidation
37 (TBARS) and total antioxidant capacity (TAOC) quantifications according to protocols already published¹⁵.
38 All assay kits for the TAOC and TBARS measurements were provided by Cayman Chemical® (US). TAOC and
39 TBARS contents were normalized to protein content following the Bradford method with serum albumin
40 standard²⁴.

41 As normality was not observed in all of the TBARS and TAOC data sets, differences between the mean
42 TBARS and TAOC levels of controls and exposed organisms at a given exposure time were assessed using a
43 non-parametric Kruskal-Wallis test, followed by a Dunn's post hoc test. Statistical analysis was performed
44 using XLStat (Addinsoft, 2010). A 5% significance ($p<0.05$) was used in all tests.

45 **Microbiota analysis**

46 Water column and sediment from the nine mesocosms were sampled at days 0 and 28. Total DNA was
47 extracted using FastDNA SPIN Kits for Soil and FastPrep-24 Instrument (MP Biomedicals®, France),
48 according to the manufacturer's instructions. Variable regions 1 to 3 (V1–V3) of bacterial 16S rRNA gene
49 were amplified with the specific primers 27Fmod (5'-AGRGTGGATCMTGGCTCAG-3') and 530R
50 (CCGCNGCNGCTGGCAC) and barcode²⁵. Polymerase chain reaction (PCR) reactions were carried out using
51 HotStarTaq Plus Master Mix Kit (Qiagen, US). PCR products tagged with unique barcode from each sample
52 were equally mixed and purified using Agencourt Ampure beads (Agencourt Bioscience®, US) and

1 sequenced by MR DNA (www.mrdnalab.com, MR DNA, US) utilizing Roche 454 FLX Titanium instruments
2 and reagents.
3 Sequence data resulting from the sequencing process were processed using a proprietary analysis pipeline
4 (www.mrdnalab.com)^{26, 27}. Sequences were trimmed of barcodes and primers, and then short sequences
5 (<200 bp), sequences with ambiguous base calls, and sequences with homopolymer runs exceeding 6 bp
6 were removed. The 16S rRNA amplicon sequence data were analyzed using QIIME2 (qiime2:2019.10.0)²⁸.
7 Sequences were demultiplexed, truncated at 370 nucleotides based on sequence quality profile (>25),
8 denoised and chimeras were removed using DADA2²⁹. Sequences were aligned using MAFFT³⁰, and were
9 used to construct a phylogeny using FastTree³¹. Taxonomy was assigned using a Naïve Bayes classifier
10 trained on the GreenGenes database (version 13_8) using trimmed sequences pre-clustered at 97% of
11 similarity. 15729 features were generated from 383931 reads from 36 samples.
12 Alpha diversity measures (observed OTUs, Chao1, Simpson, Fisher's index, and Shannon's diversity) and β
13 diversity measures (Bray-Curtis dissimilarity) were generated in MicrobiomeAnalyst³² using a subsample
14 feature table rarefied to 2 833 reads for the analysis of the whole dataset including sediments and water
15 columns and to 11 522 reads when focusing on the water column samples. For β diversity and univariate
16 analysis, data were transformed with Relative log expression (RLE)³³ and filtered (minimum count 10 for a
17 feature, 20% of prevalence, filtering of features closed to constant using 10% based inter-quartile range).
18 Venn diagrams were constructed in MetaCoMET (Metagenomics Core Microbiome Exploration Tool).
19 Statistical analyses (Kruskall-Wallis, ANOVA, PERMANOVA, PERMDIST) were performed in R ([www.r-](http://www.r-project.org)
20 [project.org](http://www.r-project.org)), MicrobiomeAnalyst, or XSTAT (2019.3.2). Db-RDA was run in Vegan. For multiple testing,
21 $p < 0.05$ was considered to be statistically significant. p -values were corrected to Q -values using the
22 Benjamini-Hochberg False Discovery Rate (FDR). We selected a nonstringent Q -value set at 0.20 to avoid
23 missing any important leads (www.biostathandbook.com). All statistical analyses were performed on 3
24 replicates of the same treatment, except for the microbial community in the water column dosed with PI-
25 Ag, for which a bloom of diatoms developed in one replicate as of Day-0. This replicate was excluded from
26 the analysis (*cf.* result section).

27 Results and Discussion

28 Relevance assessment of mesocosms mimicking a lotic ecosystem

29 To assess the similarities among mesocosms before any contamination, and their ability to mimic a lotic
30 ecosystem, we explored the composition and the diversity of the benthic and water communities in the
31 mesocosms under baseline conditions at Day 0.

32 The diversity within a community (α diversity)³⁴ was described using the number of observed and predicted
33 (Chao1) OTUs that characterize the richness of microbiomes, and the Shannon and Simpson's indexes that
34 report on the richness and evenness (equitability among microbiota communities from different
35 treatments). Based on Simpson index, a high diversity was observed in surficial sediments (from 0.985 to
36 0.993) and in water columns (from 0.792 to 0.938) of mesocosms at Day 0 (Figure S4, Table S1). The
37 percentage of total species represented in a sample (Good's coverage) ranged from 98.63 to 99.89% in
38 sediments and 98.80 to 99.58% in water column, highlighting that the majority of the bacterial
39 communities was captured. Within both benthic and aquatic communities, high values of Shannon index
40 were associated to high values of observed OTUs and Chao1, indicating that the communities were rich
41 and even (not dominated by few abundant taxa). The diversity indexes within a compartment (surficial
42 sediments or water column) did not differ between mesocosms (Kruskall-Wallis test, $p < 0.05$). As expected
43 in a natural lotic ecosystem³⁵, the diversity was significantly higher in the benthic compartment than in the
44 water column (Kruskall-Wallis test, $p < 0.017$).

45 To assess dissimilarities among communities, Bray-Curtis distance (BC) summarizing compositional
46 differences was used. The principal coordinate analysis (PCoA, Figure S5) based on BC visualizes the
47 distribution of the microbiomes from surficial sediments and water columns at Day 0. A PERMANOVA
48 based on BC demonstrated that the communities in sediments and water columns were significantly
49 different ($p < 0.001$, $R^2 = 0.409$) evidencing naturally spatial niche partitioning. The bacterial community
50 composition in surficial sediments did not differ at Day 0 among the 9 mesocosms (PERMANOVA, $R^2 = 0.242$,
51 $p = 0.582$). In the water column, excluding one mesocosm where a diatomaceous Brown Algae biofilm had
52 bloomed (Figure S6), the composition did not differ among mesocosms (PERMANOVA, $p = 0.762$, $R^2 = 0.240$).
53 The bacterial compositions of surficial sediments and water columns at Day 0 are illustrated at the class
54 level in Figure S7. In the sediments, 17 phyla-subphyla were identified, of which *BetaProteobacteria*

1 (24.8%), *Alphaproteobacteria* (22.8%), *Actinobacteria* (18.4%), *Bacteroidetes* (7.8%), *Acidobacteria* (6.6%),
2 *Cyanobacteria* (6.3%), *Gamaproteobacteria* (4.8%), *Nitrospirae* (2.5%), *DeltaProteobacteria* (1.8%),
3 *Planctomycetes* (1.6%) and *Chloroflexi* (1.1%). In the water column, *Betaproteobacteria* (35.1%),
4 *Bacteroidetes* (7.5%), *Alphaproteobacteria* (29.3%), *Actinobacteria* (12.9%), *Cyanobacteria* (4.5%),
5 *Acidobacteria* (2.8%), *Gammaproteobacteria* (2.8%), and *Planctomycetes*, *Nitrospirae*, *Chloroflexi* (1.5, 1.2
6 and 1.1 %, respectively) dominated the taxonomic diversity at the phylum/class levels. Similar community
7 composition of surficial sediments and water was already observed in a survey of microbial diversity based
8 on 16S rRNA gene sequence libraries from lotic, stream and river ecosystems³⁶. Altogether, these features
9 highlight that the mesocosms at Day 0 did not differ substantially in bacterial composition and were
10 representative of a lotic system.

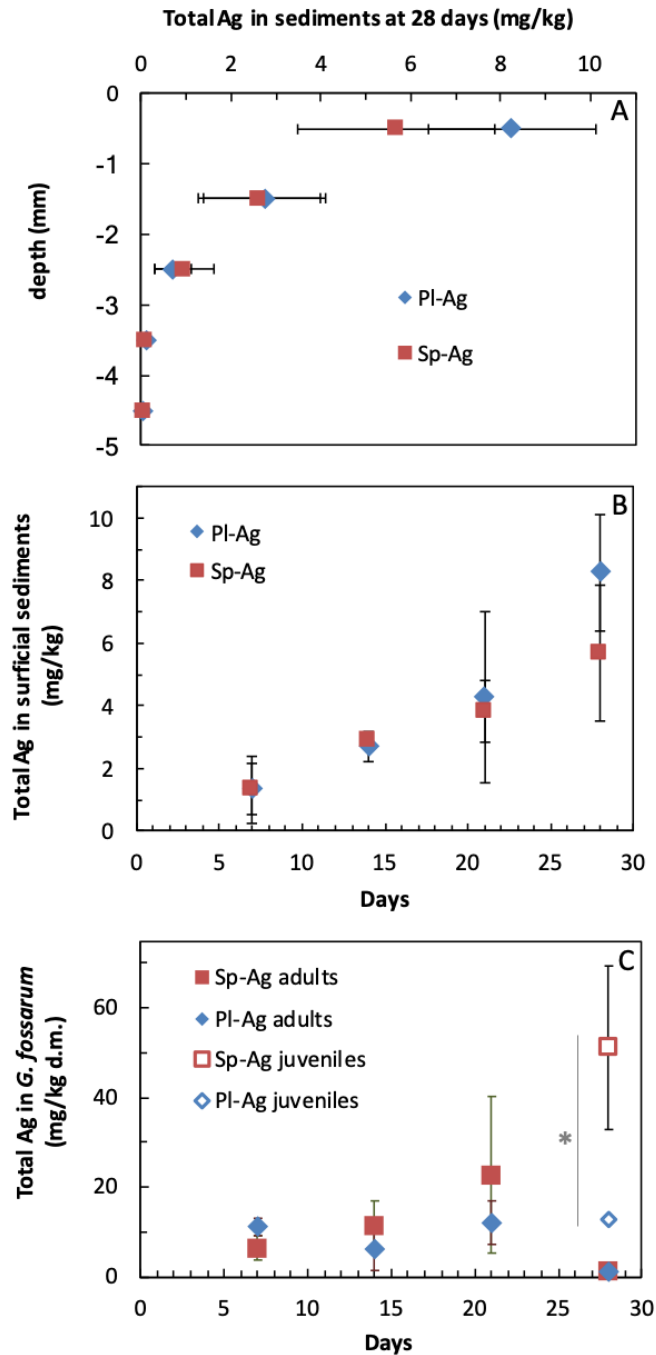
11 Benthic compartment: high exposure to Ag NMs but low impact

12 Silver accumulation in sediments and uptake by benthic organisms

13 Surficial sediments were sampled 7, 14, 21, and 28 days after the first injection of PI-Ag and Sp-Ag. An
14 increase of the Ag concentration was measured over time from $1.3 \pm 0.9 \text{ mg.kg}^{-1}$ at Day 0 to $8.3 \pm 1.9 \text{ mg.kg}^{-1}$
15 at Day 28 (Fig. 2A and Fig. 2B). No significant difference in concentrations between PI-Ag and Sp-Ag were
16 observed. Comparing the span of predicted environmental concentrations (PEC) given in the literature
17 (between 10 to $100 \mu\text{g.kg}^{-1}$) for sediments³⁷, the amount of silver measured over a month in the sediment
18 of mesocosms is two orders of magnitude higher. The analysis of cores of sediments sampled at Day 28 has
19 shown that Ag mostly accumulated in the first 3 mm of sediments (Fig. 2A). This time-dependent increase
20 of [Ag] in the sediment is attributed to the aggregation and settling of the Ag nanoparticles³⁸. The size of
21 the aggregates was evaluated in batch using Volvic® water (Figure S8). For both PI-Ag and Sp-Ag, two
22 populations of hydrodynamic diameters (d_h) were obtained after 2.5 hours centered on 40 nm and 1 500
23 nm for Sp-Ag, and on 60 nm and 1 500 nm for PI-Ag. While not measured in the water column of the
24 mesocosms, these values highlight the strong and similar aggregation expected at such pH and ionic
25 strength. This is in agreement with George et al. (2012)⁹, showing similar aggregation for PI-Ag and Sp-Ag
26 in culture media.

27 *G. fossarum* were exposed to the silver reservoir localized in the surficial sediments which represents 85 ± 19
28 % (PI-Ag) and 72 ± 34 % (Sp-Ag) of the total Ag injected. The quantity of Ag taken up or adsorbed on the
29 cuticles of adults *G. fossarum* (Fig. 2C) was not shape-dependent. It increased from $\sim 8.9 \pm 2.8 \text{ mg.kg}^{-1}$ (days
30 7 and 14) to $\sim 14.5 \pm 7.4 \text{ mg.kg}^{-1}$ (day 21) and significantly decreased to $1.3 \pm 0.1 \text{ mg.kg}^{-1}$ (day 28).
31 Concomitantly to this decrease, a significant number of juveniles *G. fossarum* was observed (Figure S9)
32 with Ag concentration of $12.8 \pm 0.1 \text{ mg.kg}^{-1}$ for PI-Ag and $51.2 \pm 18.4 \text{ mg.kg}^{-1}$ for Sp-Ag (Fig. 2C).

33 As all arthropods, female *G. fossarum* are known to shed their chitinous exoskeleton to develop, grow, and
34 spawn³⁹. The exuviation and the shedding of the chitinous cuticle and peritrophic membrane has been
35 shown as one crucial mechanism governing the release of NMs taken up in the digestive track or adsorbed
36 at the surface of arthropods⁴⁰. We hypothesize that during the last week of exposure in the mesocosms,
37 adults *G. fossarum* molt, juveniles hatched, and this exuviation induced a decrease of the Ag concentration
38 measured in adults. Hence, the [Ag] taken up was dependent on the lifecycle stages of the organisms but
39 not on the shape or even the thickness of the NMs ($\sim 20 \text{ nm}$ for the Sp-Ag and $\sim 8 \text{ nm}$ for the PI-Ag).



1

2

3

4

5

6

7

8

9

10

11

12

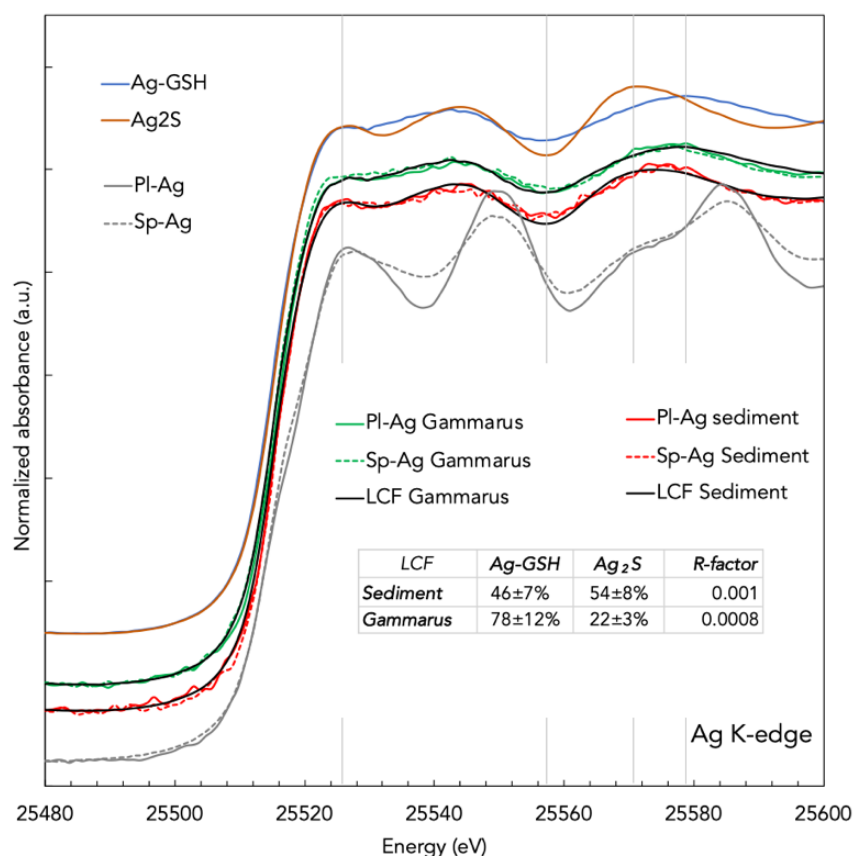
13

Fig. 2 Distribution of Ag in the sediment. (A) Total [Ag] measured in 1 mm-section of cores of sediment sampled after 4 weeks. (B) Total [Ag] measured in the surficial sediments on 0.9 ± 0.4 mm depth sampled at 7, 14, 21 and 28 days. (C) Total [Ag] taken up or adsorbed on adults *G. fossarum* sampled at 7, 14, 21 and 28 days and juveniles at 28 days. For each time point and replicate, between 3 to 10 adults and 240 to 320 juveniles were pooled prior measurement. (A, B, C) Data represent average \pm standard deviation of 3 replicated mesocosms corrected from background concentration determined in control mesocosms. * indicates a significant difference between PI-Ag and Sp-Ag ($p < 0.05$).

Ag sulfidation in the benthic compartment

It is well-known that metallic Ag is not thermodynamically stable under environmental conditions and will oxidize and/or react with (in)organic ligands as sulfide⁴¹, chloride⁴², and organic matter⁴³. The speciation of the Ag accumulated in the surficial sediments and interacting with *G. fossarum* was assessed by XANES at the Ag K-edge (Fig. 3). Metallic Ag nanoparticles have a distinct XANES signatures with high amplitude of

1 the first oscillations. Consequently, even if present in minor amounts, Ag(0) could be detected. Linear
 2 combination fitting (LCF) was performed to estimate the amount of Ag(0), Ag(I) and the nature of the first
 3 atomic shell. Herein, GSH was considered as a proxy for organic thiol-containing ligands having a strong
 4 affinity for silver (*e.g.* $\log K_{Ag-cysteine} = 11.9$), while Ag₂S was considered as a relevant highly insoluble
 5 inorganic mineral ($\log K_{Sp} = -50.2$)^{44, 45}. It is interesting to note that XANES spectra of Ag in sediment
 6 exposed to Sp-Ag and PI-Ag superimposed, as do the XANES spectra of Ag in *G. fossarum* exposed to Sp-Ag
 7 and PI-Ag (Fig. 3). The LCFs results highlight that no Ag K-edge XANES signal were attributed to Ag(0) but
 8 rather to sulfidized silver species either as inorganic bearing phase (54±8% and 22±3% respectively in
 9 sediment and *G. fossarum*) or organic Ag-thiol complex (46±7% and 78±12% respectively in sediment and
 10 *G. fossarum*). Based on the low signal/noise ratio and the fit residue, other Ag species could be present in
 11 these samples but not identified by LCFs. The XANES analysis confirmed that in freshwater organisms and
 12 sediments, silver strongly bound to both organic and inorganic sulfur likely through oxidative dissolution
 13 and precipitations⁴⁴.



14 **Fig. 3** Ag K-edge XANES spectra of Ag in the surficial sediments and taken up or adsorbed at the surface of adults *G.*
 15 *fossarum* after 28 days of exposure to Sp-Ag and PI-Ag. LCF : linear combination fits using PI-Ag, Sp-Ag, Ag-GSH, and
 16 Ag₂S reference compounds. R-factor refers to fit quality.

18 Interestingly, at Day 28, the Ag₂S/Ag-GSH ratio is lower in *G. fossarum* (~0.3) than in sediments (~1.2). This
 19 change in sulfidized species distribution could be related to pH or Eh variations, to different amount of
 20 sulfide vs. thiol-containing ligands in the sediments vs. in *G. fossarum*, but also to different bio-availabilities
 21 among Ag-S species.

22 **Low impact on benthic organisms**

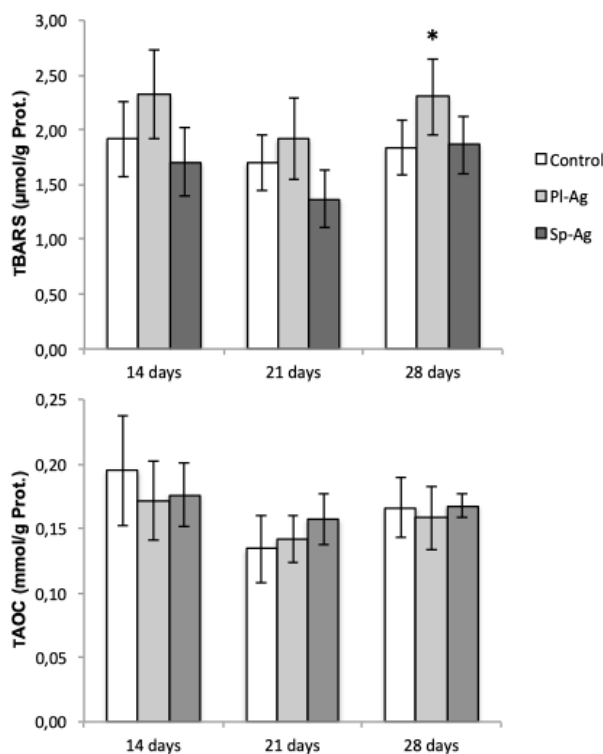
24 The impact of Sp-Ag and PI-Ag was assessed on *G. fossarum* and benthic microbial community. Regarding
 25 adults *G. fossarum*, no significant difference in the number of adults or juvenile organisms were observed
 26 between Control and Ag NMs dosed-mesocosms after 28 days (Figure S8). This confirms the absence of
 27 acute toxicity in these experimental conditions. TAOC and TBARS levels were measured before (days 14
 28 and 21) and after (day 28) the molting of *G. fossarum* (Fig. 4). No variation in TAOC was observed during
 29 the entire experiment among all treatments. However, lipid peroxidation was significantly higher ($p=0.029$)
 30 in gammarids exposed to PI-Ag after 28 days of exposure (TBARS, $2.3\pm0.4 \mu\text{mol.g}^{-1}$), compared to the

1 respective time-matched controls (TBARS, $1.8 \pm 0.3 \mu\text{mol.g}^{-1}$) (Fig. 4, and Fig. S13). A slightly lower variability
 2 in TBARS was observed in 21 and 28 days controls, and may participate to the significance of the statistical
 3 analysis observed at day 28. However, no difference between all time-matched controlled (14, 21 and 28
 4 days) was observed (Kruskall-Wallis test), which corroborate the hypothesis of the PI-Ag effect in *G.*
 5 *fossarum*. The TBARS increased concomitantly when the Ag taken up by the organisms was mainly bound
 6 to thiol-containing ligands (100% of sulfidation and $\text{Ag}_2\text{S}/\text{Ag-GSH}$ of 0.3 in *G. fossarum*, Fig. 3).
 7 Interestingly, a higher number of molting events was observed after 21 days. *Gammarus pulex*, a close-
 8 related species to *G. fossarum*, is known to be more sensitive to cadmium after molting⁴⁶. This suggests
 9 that after the exuviation occurring between day 21 and 28, *G. fossarum* could be more sensitive to Ag NMs.
 10 The higher sensitivity to PI-Ag compared to Sp-Ag is discussed in the next section.
 11 After 28 days, the richness (observed and predicted OTUs) and richness-evenness (Shannon and Simpson
 12 indexes) of the bacterial communities in the sediments were not significantly altered compared to Day 0
 13 and did not differ (Kruskall Wallis, all $p > 0.05$) showing that neither time nor exposure to PI-Ag and Sp-Ag
 14 modified the diversity in surficial sediments. At Day 28, time was the sole driver of the community
 15 composition (PERMANOVA, $p < 0.001$, $R^2 = 0.105$). Treatment and time-treatment interactions had no
 16 significant effect ($p > 0.05$) on the composition of microbiomes on the surficial sediments, showing that after
 17 28 days of chronic exposure to Sp-Ag and PI-Ag, the structure of the benthic bacterial communities
 18 remained similar to controls. These results are consistent with the sulfidation of Ag in surficial sediment
 19 (100% of sulfidation and $\text{Ag}_2\text{S}/\text{Ag-GSH}$ of ~ 1.2). Indeed, several studies have shown that Ag sulfidation
 20 reduced the impact of Ag NMs on living organisms as zebrafish, killifish, nematode worms, microbial
 21 communities *etc.*^{20, 47-49}. This was due to the lower solubility of sulfidized Ag relative to metallic Ag and
 22 consequently the lowest release of ecotoxic dissolved silver species following sulfidation.

23 Planktonic compartment: low exposure to Ag NMs but significant impacts on microbial community

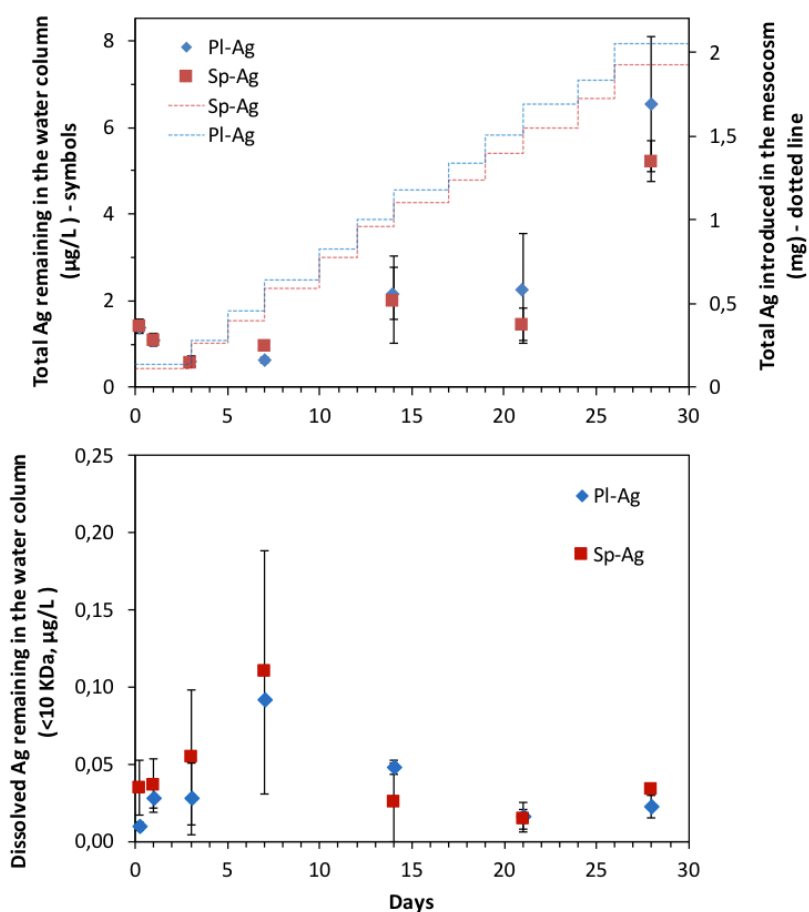
24 Silver behavior and speciation in the water column.

25 During 4 weeks, the total and dissolved (<10 kDa) amount of silver were measured in the water column
 26 (Fig. 5). Each sampling, except between Day 0 and Day 3, were performed few minutes before the following
 27 dosing. Thus, these concentrations correspond the amount of silver remaining in the water column after
 28 all bio-physical-chemical transformations occurred (*e.g.* aggregation, uptake, ...).



29
 30 **Fig. 4** Lipid peroxidation (TBARS) and total antioxidant capacity (TOAC) in *G. fossarum*. Value are means \pm sd. *
 31 indicates a significant difference with the respective control group ($p < 0.05$).

1 In all cases, no significant difference in the means of total [Ag] or dissolved [Ag] in the water column was
 2 observed following Sp-Ag and PI-Ag contaminations. The total [Ag] increased from $1.4 \pm 0.2 \mu\text{g.L}^{-1}$ at Day 3
 3 (for both PI-Ag and Sp-Ag) to $6.5 \pm 1.5 \mu\text{g.L}^{-1}$ for PI-Ag and $5.2 \pm 0.5 \mu\text{g.L}^{-1}$ for Sp-Ag at Day 28. Comparing the
 4 span of PEC given in the literature (between 10^{-5} to $10^{-1} \mu\text{g.L}^{-1}$) for surface waters³⁷ to the amount of silver
 5 measured over a month in the water column of the mesocosms, provides an indication of the
 6 environmental relevance of these experiments. The linear decrease ($R=0.99$) observed between Day 0 and
 7 Day 3 shows the fast removal of silver from the water column between two dosing's. We estimated that
 8 after 5h and 72h, respectively 54% and 80% of the silver was removed. This was similar to the kinetics of
 9 removal already measured for (un)coated CeO_2 NMs despite their different physical-chemical mechanisms
 10 of solubility (reductive dissolution for CeO_2 vs. oxidative dissolution for metallic Ag)¹⁴. At the end of the
 11 experiment, a mass balance calculation shows that less than 15% of silver remained in the water column.
 12 Mathematical integration of the dissolved [Ag] in the water column over time allowed to calculate a
 13 theoretical total exposure concentration over one month to dissolved Ag of $0.12 \pm 0.05 \mu\text{g.L}^{-1} \cdot \text{month}^{-1}$ for
 14 PI-Ag and $0.17 \pm 0.08 \mu\text{g.L}^{-1} \cdot \text{month}^{-1}$ for Sp-Ag. Specifically, the mesocosms were observed to evolve over
 15 two distinct periods of time independently of the Ag NMs shape (Fig. 5) : dissolved [Ag] increased during
 16 the first week to $\sim 0.10 \mu\text{g.L}^{-1}$ and then decreased and stabilized around $\sim 0.025 \mu\text{g.L}^{-1}$. We hypothesized
 17 that these two periods were attributed to (i) the oxidative dissolution of Ag(0) and (ii) the precipitation of
 18 the silver species in solution. Based on the solubility products (e.g. $K_{\text{sp}} \text{Ag}_2\text{O} = 4 \times 10^{-11}$ versus $K_{\text{sp}} \text{Ag}_2\text{S} =$
 19 5.92×10^{-51}), speciation determine by XANES, and the cationic/anionic composition of the water column,
 20 silver sulfidation is the most favorable transformation leading to this precipitation⁵⁰.



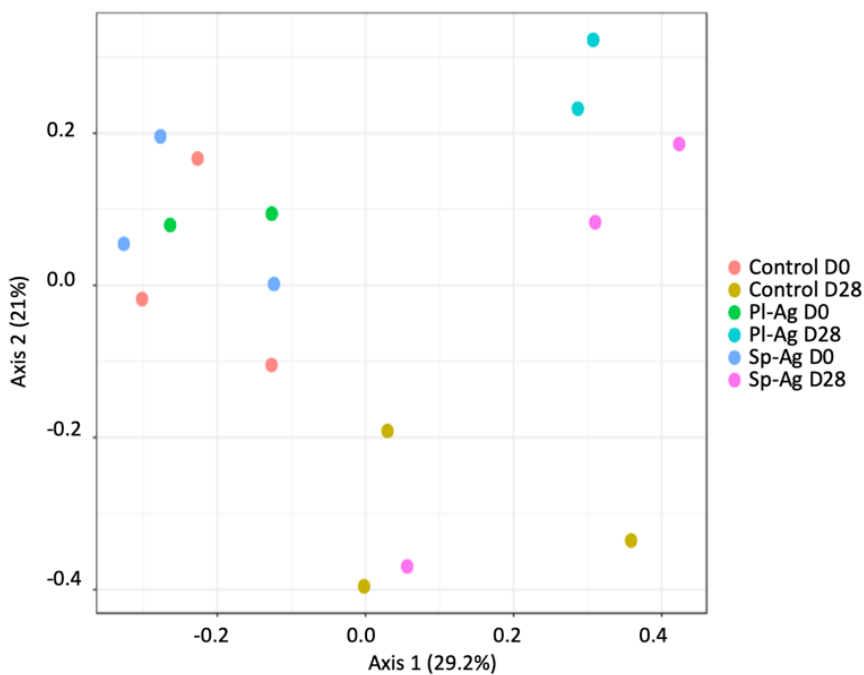
21
 22 **Fig. 5** Distribution of Ag in the water column. (top) Total [Ag] injected in the mesocosms (dotted lines) and dosed
 23 in the water column (symbols). The water was sampled at 10 cm from the air/water interface. (bottom) Dissolved
 24 [Ag] (<10 kDa). Data represent average \pm standard deviation ($n = 3$) corrected from background concentration
 25 determined in control mesocosms. No significant difference between PI-Ag and Sp-Ag was observed ($p < 0.05$).

26 **Significant impacts on planktonic microbial community.**

1 The impact of PI-Ag and Sp-Ag on the bacterial microbiomes diversity and composition in the water column
2 was assessed by sequencing of 16S rRNA gene amplicons. After 28 days, all indicators of diversity did not
3 differ among treatments (Kruskal-Wallis test, $p>0.05$) (Figure S10, Table S2). As compared to Day 0,
4 observed OTUs and Chao1 at D28 were significantly lower in the PI-Ag dosed mesocosms ($p<0.05$), but not
5 the Shannon and Simpson indexes ($p>0.05$), showing that the water columns differed in terms of richness
6 but not in terms of effective diversities. The Sp-Ag treatment did not significantly affect the diversity in the
7 water column over the 28 days of exposure.

8 Ordination based on the BC distance matrix (PCoA, Fig. 6) shows the distribution of the microbiomes in the
9 water column of the mesocosms at days 0 and 28, for the different treatments. A PERMANOVA showed
10 that among the explicative variables, the treatment-time interaction ($R^2= 0.510$, $p<0.007$) and the time
11 (PERMANOVA, $R^2= 0.245$, $p<0.001$) were the main drivers of the community composition. Between days 0
12 and 28, all controls shifted and clustered downwards and to the right, while the Ag NMs-dosed
13 communities (PI-Ag and Sp-Ag) shifted upwards and to the right. Note that the mesocosm in which a
14 diatomaceous Brown Algae biofilm had bloomed and differed from the other mesocosms as of Day-0, was
15 excluded from the dataset.

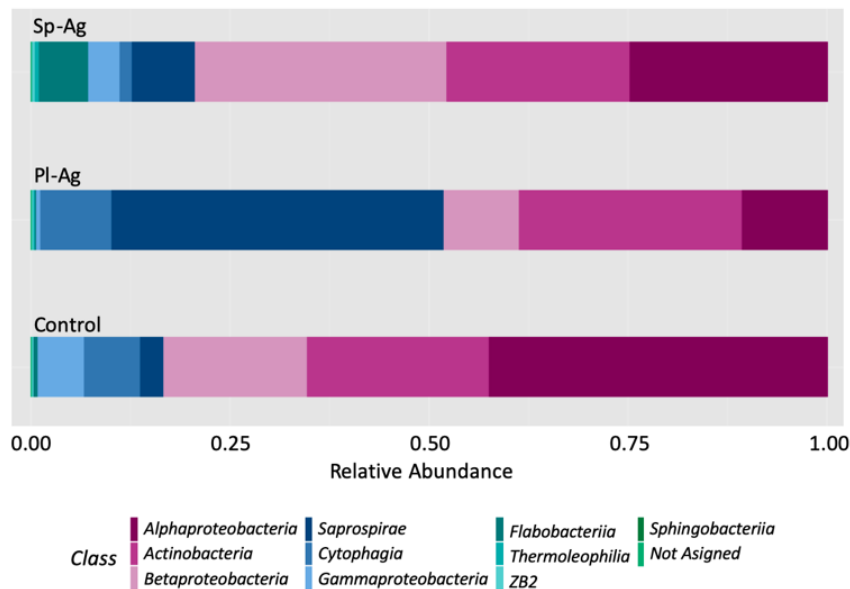
16



17

18 **Fig. 6** Principal coordinate analysis based on Bray Curtis dissimilarity of microbiomes in the water column (WC).
19 Microbiomes are visualized at Day 0 (D0) and Day 28 (D28), respectively for Control mesocosms (coral and gold
20 dots), PI-Ag exposed mesocosms (green and cyan dots) and Sp-Ag treated mesocosms (blue and pink dots).

21 At D28 in the water column, a PERMANOVA on BC distance matrix showed a significant clustering based
22 on treatment ($p<0.037$, $R^2=0.467$). Univariate analysis showed differences at OTU and all taxonomic levels,
23 illustrated at the class-level (Fig. 7). No significant difference in composition was detected between the
24 water column composition of Sp-Ag dosed- and Control-mesocosms ($FDR>0.20$). However, the composition
25 of the bacterial communities from the water column was significantly altered by PI-Ag at the phylum level,
26 with a 5-fold increase in the relative abundance of *Bacteroidetes* ($p=0.0029$, $FDR=0.011$) and a 3-fold
27 decrease in *Proteobacteria* ($p=0.069$, $FDR<0.139$). At the order level, a 15-fold increase was observed in
28 *Saprospirales* ($p<0.0009$, $FDR=0.017$) in PI-Ag-dosed vs Controls. At the genus level, a 23-fold increase in a
29 genus related to *Sediminibacterium* in the PI-Ag vs Control ($p<0.0008$; $FDR<0.017$). *Sediminibacterium*
30 genus has been described in sediment biofilms and in the water column of streams⁵¹.



1
2 **Fig. 7** Mean abundances at the class-level of the water bacterial community after 28 days in the mesocosms exposed
3 to PI-Ag, Sp-Ag and Controls.

4 **Can the shift of microbiomes exposed to Ag NMs be understood in terms of toxicity?**

5 To understand whether this change in abundance is a marker of toxicity, ecological patterns were sought
6 out focusing on the dynamic core microbiome⁵². The consistently detected or persistent core microbiome
7 was defined by taxa that were present within a user-specified fraction (0.8) of the samples to be counted
8 as belonging to that group. Persistent core microbiomes are postulated to be responsible for microbially
9 driven ecosystem processes, as illustrated in the ocean water column⁵³. Spatial or temporal samplings allow
10 for identification of spatially- (*i.e.* over different replicates of a same treatment) or temporally-dynamic
11 persistent core microbiomes.

12 At Day 0, 14 OTUs were consistently shared as a spatial persistent core microbiome among the water
13 columns of the mesocosms. These persistent spatially core microbiome taxa represented on average 56%,
14 47% and 46% of the total community abundance for Control, PI-Ag and Sp-Ag-dosed mesocosms
15 respectively (Figure S11). At Day 28, the number of consistent OTUs among mesocosms decreased to 6
16 persistent taxa showing a shrink in the core microbiome as a result of time and Ag NMs treatment *i.e.* a
17 system divergence. The abundance of core microbiome taxa after 28 days decreased to 35% and 21% of
18 the total abundance for Control and Sp-Ag-dosed mesocosms, but increased to 54% for PI-Ag exposed
19 mesocosms (Figure S12).

20 Within each treatment, we compared the temporally dynamic core microbiome based on persistence.
21 Between days 0 and 28, the persistent core microbiome was richer in the mesocosms exposed to PI-Ag
22 with 15 OTUs than 8 OTUs for Sp-Ag and 7 taxa for Controls. In all cases, the response of the bacterial
23 community to time and Ag NMs treatments went through an increase in the total core microbiome
24 abundance vs. the total bacterial community and a modulation of the taxa abundance within the core
25 community (Figure S11). Together, these patterns suggest rather a stimulation of microbial communities
26 due to PI-Ag than a toxic effect.

27 **Environmental implications**

28 Our results point out shape-dependent impacts towards organisms and communities living in a lotic
29 ecosystem. Despite similar behavior (dissolution, aggregation, Fig. 2, Fig. 5), Sp-Ag impacted neither the
30 benthic macro-organisms nor the microbial communities, while PI-Ag induced a moderate oxidative stress
31 in adult *G. fossarum* (Fig. 4) and destabilized the planktonic microbial communities (Fig. 6, Fig. 7).
32 Interestingly, the shift of microbiota in the water column in response to PI-Ag points to an hormesis effect
33 instead of a toxic event towards the community. Such a stimulation was already observed in term of growth
34 of *Cupriavidus necator* at low Ag NMs concentrations⁵⁴, as well as in *Pseudomonas aeruginosa* exposed to
35 20 mg.L⁻¹ Ag NMs⁵⁵. A shape-dependent biological responses to Ag NMs was already observed *in vitro*
36 toward fish gill cells, red blood cells, zebrafish embryos⁹, and *E. coli*¹⁰. The high levels of defects at the

1 surface of PI-Ag⁹ associated with the high reactivity of the edges and corners of triangular-shaped NPs
2 might be responsible for the alteration of biomolecules or cellular structures *via* direct contact and
3 generation of free oxygen radicals. This could explain the presence of oxidative damage and the shift in the
4 microbial communities observed with PI-Ag herein.

5 From an environmental risk perspective, our results highlight which ecological niches of a lotic
6 ecosystems would be more impacted by PI-Ag. Indeed, despite the highest exposure to Ag NMs in the
7 benthic compartment (surficial sediment), the biological impacts were lower than in the planktonic
8 compartment. These results confirm what has been recently stated by the scientific community, *i.e.* that
9 the speciation and transformation of NMs rather than their concentrations drive the biological responses.
10 Indeed, the surficial sediment contained >72% of the total Ag injected after 1 month, however the Ag is
11 fully sulfidized and consequently less available to significantly impact the macro-and micro-organisms (only
12 moderate effect were observed on *G. fossarum*). However, even if only 11 to 15% of the Ag remained in
13 the water column after 1 month, Ag is present as a more reactive species (likely less oxidized surface of
14 NMs and dissolved species) and more significantly impacts the pelagic community.

15 From a safer by design perspective, Falinski et al. (2018) proposed a framework for sustainable NMs
16 selection and design based on (1) performance, (2) hazard, and (3) economic considerations⁵⁶. The current
17 paper did not intend to inform about (1) and (3), but focus on the environmental footprint (2) of Ag NMs
18 based on their shape. The results presented herein could inform decision-making for the implementation
19 of Ag NMs by maximizing the ratio of NMs functional performance (*e.g.* antibacterial, optical, electric
20 properties) to environmental risks (shape-dependent effects).

21 Conflicts of interest

22 There are no conflicts to declare.

23 Acknowledgements

24 The authors thank the CNRS for funding the IRP iNOVE, and the French ANR for funding the ANR-10-NANO-
25 0006/MESONNET project. The authors acknowledge financial support provided by the FP7
26 project NANoREG (A common European approach to the regulatory testing of Manufactured
27 Nanomaterials; European Commission, Grant Agreement Number 310584). This work has received funding
28 from Excellence Initiative of Aix - Marseille University - A*MIDEX, a French “Investissements d'Avenir”
29 program, through its associated Labex SERENADE project. This work is also a contribution to the OSU-
30 Institut Pythéas.

31 References

- 32 1. Y. Sun and Y. Xia, *Science*, 2002, **298**, 2176+.
- 33 2. M. Auffan, J. Rose, J. Y. Bottero, G. Lowry, J. P. Jolivet and M. R. Wiesner, *Nature Nanotechnology*,
34 2009, **4**, 634-641.
- 35 3. M. E. Vance, T. Kuiken, E. P. Vejerano, S. P. McGinnis, M. F. Hochella, Jr., D. Rejeski and M. S. Hull,
36 *Beilstein Journal of Nanotechnology*, 2015, **6**, 1769-1780.
- 37 4. S. Foss Hansen, L. R. Heggelund, P. Revilla Besora, A. Mackevica, A. Boldrin and A. Baun,
38 *Environmental Science: Nano*, 2016, **3**, 169-180.
- 39 5. M. O. Gorbunova, A. V. Shevchenko, V. V. Apyari, A. A. Furletov, P. A. Volkov, A. V. Garshev and S.
40 G. Dmitrienko, *Sensors and Actuators B: Chemical*, 2018, **256**, 699-705.
- 41 6. Z. Wang, F. Liao, T. Guo, S. Yang and C. Zeng, *Journal of Electroanalytical Chemistry*, 2012, **664**, 135-
42 138.
- 43 7. R. M. Anuj, K. Akshay and Z. Chongwu, *Nanotechnology*, 2011, **22**, 245201.
- 44 8. R. Xu, D. Wang, J. Zhang and Y. Li, *Chemistry – An Asian Journal*, 2006, **1**, 888-893.
- 45 9. S. George, S. Lin, Z. Ji, C. R. Thomas, L. J. Li, M. Mecklenburg, H. Meng, X. Wang, H. Zhang, T. Xia, J.
46 N. Hohman, S. Lin, J. I. Zink, P. S. Weiss and A. E. Nel, *ACS Nano*, 2012, **6**, 3745–3759.
- 47 10. S. Pal, Y. K. Tak and J. M. Song, *Appl. Environ. Microbiol.*, 2007, **73**, 1712-1720.
- 48 11. Y. K. Tak, S. Pal, P. K. Naoghare, S. Rangasamy and J. M. Song, *Scientific Reports*, 2015, **5**, 16908.
- 49 12. G. Morose, *Journal of Cleaner Production*, 2010, **18**, 285-289.

- 1 13. M. Auffan, W. Liu, L. Brousset, L. Scifo, A. Pariat, M. Sanles, P. Chaurand, B. Angeletti, A. Thiery, A.
2 Masion and J. Rose, *Environmental Science: Nano*, 2018, **5**, 2579-2589.
- 3 14. M. Tella, M. Auffan, L. Brousset, E. Morel, O. Proux, C. Chaneac, B. Angeletti, C. Pailles, E. Artells, C.
4 Santaella, J. Rose, A. Thiery and J.-Y. Bottero, *Environmental Science: Nano*, 2015, **2**, 653-663.
- 5 15. M. Tella, M. Auffan, L. Brousset, J. Issartel, I. Kieffer, C. Pailles, E. Morel, C. Santaella, B. Angeletti,
6 E. Artells, J. Rose, A. Thiery and J.-Y. Bottero, *Environmental Science & Technology*, 2014, **48**, 9004-
7 9013.
- 8 16. M. Auffan, M. Tella, C. Santaella, L. Brousset, C. Pailles, M. Barakat, B. Espinasse, E. Artells, J. Issartel,
9 A. Masion, J. Rose, M. Wiesner, W. Achouak, A. Thiery and J.-Y. Bottero, *Scientific reports*, 2014, **4**,
10 5608.
- 11 17. M. Auffan, A. Masion, C. Mouneyrac, C. de Garidel-Thoron, C. O. Hendren, A. Thiery, C. Santaella, L.
12 Giamberini, J.-Y. Bottero, M. R. Wiesner and J. Rose, *NanoImpact*, 2019, **13**, 66-69.
- 13 18. G. S. Karaman and S. Pinkster, *Bijdr. Dierk 1977*, **47**, 1-97.
- 14 19. K. Mehennaoui, A. Georgantzopoulou, V. Felten, J. Andreï, M. Garaud, S. Cambier, T. Serchi, S. Pain-
15 Devin, F. Guérol, J.-N. Audinot, L. Giambérini and A. C. Gutleb, *Science of The Total Environment*,
16 2016, **566-567**, 1649-1659.
- 17 20. M. Auffan, C. Matson, J. Rose, M. Arnold, O. Proux, B. Fayard, P. Chaurand, M. R. Wiesner, J.-Y.
18 Bottero and R. Di Giulio, *Nanotoxicology*, 2014, **8**, 167-176
- 19 21. O. Proux, X. Biquard, E. Lahera, J.-J. Menthonnex, A. Prat, O. Ulrich, Y. Soldo, P. Evisson, G.
20 Kapoujyan, G. Perroux, P. Taunier, D. Grand, P. Jeantet, M. Deleglise, J.-P. Roux and J. L. Hazemann,
21 *Phys. Scr.*, 2005, **T115**, 970-973.
- 22 22. O. Proux, V. Nassif, A. Prat, O. Ulrich, E. Lahera, X. Biquard, J.-J. Menthonnex and J.-L. Hazemann, *J.*
23 *Synchrotron Radiat.*, 2006, **13**, 59-68.
- 24 23. B. Ravel and M. Newville, *J. Synchrotron Radiat.*, 2005, **12**, 537-541.
- 25 24. M. M. Bradford, *Anal. Biochem.*, 1976, **72**, 248-254.
- 26 25. S. E. Dowd, T. R. Callaway, R. D. Wolcott, Y. Sun, T. McKeenan, R. G. Hagevoort and T. S. Edrington,
27 *BMC Microbiol*, 2008, **8**, 125.
- 28 26. D. Nagy-Szakal, M. C. Ross, S. E. Dowd, S. A. V. Mir, T. D. Schaible, J. F. Petrosino and R. Kellermayer,
29 *Gut Microbes*, 2012, **3**, 426-433.
- 30 27. T. S. Edrington, S. E. Dowd, R. F. Farrow, G. R. Hagevoort, T. R. Callaway, R. C. Anderson and D. J.
31 Nisbet, *Journal of Dairy Science*, 2012, **95**, 4519-4525.
- 32 28. E. Bolyen, J. R. Rideout, M. R. Dillon, N. A. Bokulich, C. C. Abnet, G. A. Al-Ghalith, H. Alexander, E. J.
33 Alm, M. Arumugam, F. Asnicar, Y. Bai, J. E. Bisanz, K. Bittinger, A. Brejnrod, C. J. Brislawn, C. T.
34 Brown, B. J. Callahan, A. M. Caraballo-Rodríguez, J. Chase, E. K. Cope, R. Da Silva, C. Diener, P. C.
35 Dorrestein, G. M. Douglas, D. M. Durall, C. Duvallet, C. F. Edwardson, M. Ernst, M. Estaki, J. Fouquier,
36 J. M. Gauglitz, S. M. Gibbons, D. L. Gibson, A. Gonzalez, K. Gorlick, J. Guo, B. Hillmann, S. Holmes, H.
37 Holste, C. Huttenhower, G. A. Huttley, S. Janssen, A. K. Jarmusch, L. Jiang, B. D. Kaehler, K. B. Kang,
38 C. R. Keefe, P. Keim, S. T. Kelley, D. Knights, I. Koester, T. Kosciulek, J. Kreps, M. G. I. Langille, J. Lee,
39 R. Ley, Y.-X. Liu, E. Loftfield, C. Lozupone, M. Maher, C. Marotz, B. D. Martin, D. McDonald, L. J.
40 McIver, A. V. Melnik, J. L. Metcalf, S. C. Morgan, J. T. Morton, A. T. Naimey, J. A. Navas-Molina, L. F.
41 Nothias, S. B. Orchanian, T. Pearson, S. L. Peoples, D. Petras, M. L. Preuss, E. Priesse, L. B.
42 Rasmussen, A. Rivers, M. S. Robeson, P. Rosenthal, N. Segata, M. Shaffer, A. Shiffer, R. Sinha, S. J.
43 Song, J. R. Spear, A. D. Swafford, L. R. Thompson, P. J. Torres, P. Trinh, A. Tripathi, P. J. Turnbaugh,
44 S. Ul-Hasan, J. J. J. van der Hooft, F. Vargas, Y. Vázquez-Baeza, E. Vogtmann, M. von Hippel, W.
45 Walters, Y. Wan, M. Wang, J. Warren, K. C. Weber, C. H. D. Williamson, A. D. Willis, Z. Z. Xu, J. R.
46 Zaneveld, Y. Zhang, Q. Zhu, R. Knight and J. G. Caporaso, *Nature Biotechnology*, 2019, **37**, 852-857.
- 47 29. B. J. Callahan, P. J. McMurdie, M. J. Rosen, A. W. Han, A. J. A. Johnson and S. P. Holmes, *Nature*
48 *Methods*, 2016, **13**, 581-583.
- 49 30. K. Katoh and D. M. Standley, *Molecular Biology and Evolution*, 2013, **30**, 772-780.
- 50 31. M. N. Price, P. S. Dehal and A. P. Arkin, *Molecular Biology and Evolution*, 2009, **26**, 1641-1650.
- 51 32. J. Chong, P. Liu, G. Zhou and J. Xia, *Nature Protocols*, 2020, **15**, 799-821.
- 52 33. S. Anders and W. Huber, *Nature Precedings*, 2010, DOI: 10.1038/npre.2010.4282.2.

- 1 34. R. H. Whittaker, *Taxon*, 1972, **21**, 213-251.
- 2 35. T. Liu, A. N. Zhang, J. Wang, S. Liu, X. Jiang, C. Dang, T. Ma, S. Lui, Q. Chen, S. Xie, T. Zhang and J. Ni,
3 *Microbiome*, 2018, **6**, 16.
- 4 36. L. H. Zeglin, *Frontiers in microbiology*,, 2015, **6**, 454.
- 5 37. F. Gottschalk, T. Sun and B. Nowack, *Environmental Pollution*, 2013, **181**, 287-300.
- 6 38. G. V. Lowry, B. P. Espinasse, A. R. Badireddy, C. J. Richardson, B. C. Reinsch, L. D. Bryant, A. J. Bone,
7 A. Deonarine, S. Chae, M. Therezien, B. P. Colman, H. Hsu-Kim, E. S. Bernhardt, C. W. Matson and
8 M. R. Wiesner, *Environmental Science & Technology*, 2012, **46**, 7027-7036.
- 9 39. M. Pockl, B. W. Webb and D. W. Sutcliffe, *Freshwater biology*, 2003, **48**, 53-66.
- 10 40. M. Auffan, D. Bertin, P. Chaurand, C. Pailles, C. Dominici, J. Rose, J.-Y. Bottero and A. Thiery, *Water
11 Research*, 2013, **47**, 3921-3930.
- 12 41. C. Levard, B. C. Reinsch, F. M. Michel, C. Oumahi, G. V. Lowry and G. E. J. Brown, *Environmental
13 Science & Technology*, 2011, **45**, 5260-5266.
- 14 42. C. Levard, S. Mitra, T. Yang, A. D. Jew, A. R. Badireddy, G. V. Lowry and G. E. Brown, *Environmental
15 Science & Technology*, 2013, **47**, 5738-5745.
- 16 43. S. M. Wirth, G. V. Lowry and R. D. Tilton, *Environmental Science & Technology*, 2012, **46**, 12687-
17 12696.
- 18 44. C. Levard, E. M. Hotze, G. V. Lowry and G. E. Brown, *Environmental Science & Technology*, 2012, **46**,
19 6900-6914.
- 20 45. C. Larue, H. Castillo-Michel, S. Sobanska, L. Cécillon, S. Bureau, V. Barthès, L. Ouerdane, M. Carrière
21 and G. Sarret, *Journal of Hazardous Materials*, 2014, **264**, 98-106.
- 22 46. C. P. McCahon and D. Pascoe, *Freshwater Biology* 1988, **19**, 197-203.
- 23 47. C. Levard, E. M. Hotze, B. P. Colman, A. L. Dale, L. Truong, X. Y. Yang, A. J. Bone, G. E. Brown, R. L.
24 Tanguay, R. T. Di Giulio, E. S. Bernhardt, J. N. Meyer, M. R. Wiesner and G. V. Lowry, *Environmental
25 Science & Technology*, 2013, **47**, 13440-13448.
- 26 48. J. Meyer, C. A. Lord, X. Y. Yang, E. A. Turner, A. R. Badireddy, S. M. Marinakos, A. Chilkoti, M. Wiesner
27 and M. Auffan, *Aquat. Toxicol.*, 2010, **100**, 140-150.
- 28 49. C. L. Doolette, V. V. S. R. Gupta, Y. Lu, J. L. Payne, D. J. Batstone, J. K. Kirby, D. A. Navarro and M. J.
29 McLaughlin, *PloS one*, 2016, **11**, e0161979-e0161979.
- 30 50. M. Pourbaix, *Atlas of electrochemical equilibria in aqueous solutions*, National Association of
31 Corrosion Engineers, Houston, Texas, 1974.
- 32 51. K. Besemer, H. Peter, J. B. Logue, S. Langenheder, E. S. Lindström, L. J. Tranvik and T. J. Battin, *The
33 ISME journal*, 2012, **6**, 1459-1468.
- 34 52. J. R. Björk, R. B. O'Hara, M. Ribes, R. Coma and J. M. Montoya, *bioRxiv*, 2018, DOI: 10.1101/137885,
35 137885.
- 36 53. D. R. Mende, D. Boeuf and E. F. DeLong, *Frontiers in Microbiology*, 2019, **10**.
- 37 54. V. J. Schacht, L. V. Neumann, S. K. Sandhi, L. Chen, T. Henning, P. J. Klar, K. Theophel, S. Schnell and
38 M. Bunge, *Journal of Applied Microbiology*, 2013, **114**, 25-35.
- 39 55. D. E. Gorka, J. S. Osterberg, C. A. Gwin, B. P. Colman, J. N. Meyer, E. S. Bernhardt, C. K. Gunsch, R.
40 T. DiGulio and J. Liu, *Environmental Science & Technology*, 2015, **49**, 10093-10098.
- 41 56. M. M. Falinski, D. L. Plata, S. S. Chopra, T. L. Theis, L. M. Gilbertson and J. B. Zimmerman, *Nature
42 Nanotechnology*, 2018, **13**, 708-714.
- 43
- 44